Available online at www.sciencedirect.com
ScienceDirect
Polymer 48 (2007) 7345–7355
polymer
www.elsevier.com/locate/polymer

Dynamics of single-walled carbon nanotube (SWNT)/polyisoprene (PI) nanocomposites in electric and mechanical fields

HyungKi Lee [a], Srdjan Pejanović [b], Iñaki Mondragon [c], Jovan Mijović [a,*]

[a] *Othmer-Jacobs Department of Chemical and Biological Engineering, Polytechnic University, Six Metrotech Center, Brooklyn, NY 11201, USA*
[b] *Faculty of Technology, University of Belgrade, Karnegijeva 4, Belgrade 11000, Serbia*
[c] *University of the Basque Country, Donostia-San Sebastian 21000, Spain*

Received 12 July 2007; received in revised form 4 October 2007; accepted 5 October 2007
Available online 12 October 2007

Abstract

Relaxation dynamics of single-walled carbon nanotube (SWNT)/polyisoprene (PI) nanocomposites were examined by dielectric relaxation spectroscopy (DRS) and dynamic mechanical spectroscopy (DMS) over a wide range of frequency and temperature. Both functionalized (SWNT-f) and pristine (SWNT-p) nanotubes were used and their effect on dynamics compared. Functionalized (PISF) nanocomposites were characterized by an increase in the time scale of *the normal mode process* as a consequence of the strong surface interactions between the polymer matrix and the nanotubes. The exact opposite is seen in pristine (PISP) nanocomposites where a decrease in the time scale of the normal mode relaxation is observed and attributed to weaker surface interactions and the effect of confinement on dynamics. *The segmental process* in PISF or PISP is not affected by the presence of nanotubes. The temperature dependence of the average relaxation time for normal and segmental modes is of the Vogel–Fulcher–Tammann (VFT) type. A good agreement is observed in the time scale of processes measured by DRS and DMS in PISF nanocomposites. In PISP nanocomposites, however, the time scales obtained from DRS and DMS measurements are not in consistently good agreement and an explanation is offered in terms of confinement.

Keywords: Polyisoprene; Single-walled carbon nanotubes; Dielectric relaxation spectroscopy

1. Introduction

Single-walled carbon nanotube (SWNT) based polymer nanocomposites are of considerable current interest to scientists and engineers because of their unique physical and mechanical properties that are not attainable with conventional composites [1,2]. As a class of materials, carbon nanotube polymer nanocomposites are young [3] and the interested reader is referred to a recent comprehensive review of the most significant accomplishment in the field [4].

Enhancement of properties upon the addition of nanofillers depends on the processing method (melt mixing, solvent-based blending, in situ polymerization, etc.), good dispersion of nanofillers and optimum interactions between the nanofillers and the polymer matrix [5–9]. Good compatibility between the nanofillers and the polymer matrix is important [10,11]. SWNTs are fiber-like nanofillers with high aspect ratio (~1000), strong conductance and large interfacial area that is conducive to good dispersion in the polymer matrix. Covalent or non-covalent attachment of functional groups to SWNTs has been utilized to (1) improve compatibility and dispersion of SWNTs in the polymer matrix, and (2) enhance interfacial interactions between the filler and the matrix [12,13]. For example, Tour et al. [14] investigated mechanical properties of SWNT/polystyrene nanocomposites and showed that the small strain oscillatory behavior is strongly influenced by dispersion of functionalized nanofillers.

The presence of dispersed nanotubes raises the question of confinement and its effect on dynamics. Previous studies of dynamics in confined spaces have focused largely on thin films

* Corresponding author. Tel.: +1 718 2603097; fax: +1 718 2603125.
E-mail address: jmijovic@poly.edu (J. Mijović).

0032-3861/$ - see front matter © 2007 Elsevier Ltd. All rights reserved.
doi:10.1016/j.polymer.2007.10.011

or nanopores and have yielded controversial results with regard to the effect of confinement on the time scale of normal and segmental mode relaxation. Here we report on how dispersed SWNTs affect molecular motion of polymer matrix chains in electric and mechanical fields and what role surface functionalization and loading play. We focus on dynamics because one must understand molecular motions in nanocomposites in order to realize the macroscopic properties of these materials from molecular concepts. When placed in an electric field, polymer nanocomposites are polarized by translational and/or orientational motions of ions, interfacial charges and dipoles. Those polarization mechanisms have different time scales, making dielectric spectroscopy, with its unmatched frequency window, a particularly attractive technique for the study of nanocomposite dynamics.

The combined use of dielectric relaxation spectroscopy (DRS) and dynamic mechanical spectroscopy (DMS) to probe the dynamics of SWNT/polymer nanocomposites has not been systematically explored before this study. Our principal objective is to explore the effect of surface functionalization and loading on the dielectric and rheological behavior of pristine (PISP) and functionalized (PISF) nanocomposites.

2. Experimental

2.1. Materials

1,4-*cis*-Polyisoprene homopolymer ($M_w = 26{,}900$ g/mol; $M_w/M_n = 1.07$) was synthesized in the laboratory of Professor Jimmy Mays at the University of Tennessee and was used as polymer matrix in all nanocomposites. AP grade SWNTs (diameter × length: 1.2–1.5 nm × 2–5 μm, bundles, purity of 70%) were obtained from Carbolex and used without further purification. Chemicals used for functionalization of SWNTs were purchased from Sigma–Aldrich.

2.2. Functionalization of SWNTs

An aniline derivative was used to covalently attach functional groups on the nanotube walls. SWNTs were first mixed with a surfactant (1,2-dichlorobenzene) and sonicated for 10 min. Aniline derivative (2-methylthio-aniline) in acetonitrile was added to the SWNT solution while purging with nitrogen. Next, isopentyl nitrite was added to the solution. The homogenized solution was maintained in a screw-capped bottle and stirred continuously for 16 h at constant temperature (60 °C). During functionalization, the diazonium species were covalently bonded to SWNT side walls (Scheme 1) [15]. The excess nitrogen evolved in the early stage of reaction was removed by slightly opening the cap every hour in order to prevent the build-up of pressure inside the bottle. When the reaction was over, the solution was diluted with dimethylformamide (DMF) and filtered through a nylon membrane (0.45 μm). The collected solid was washed with DMF until the filtrate became colorless. DMF was removed by washing with ether and drying in a vacuum oven overnight. The codes used throughout the text for functionalized and pristine nanotubes are SWNT-f and SWNT-p, respectively.

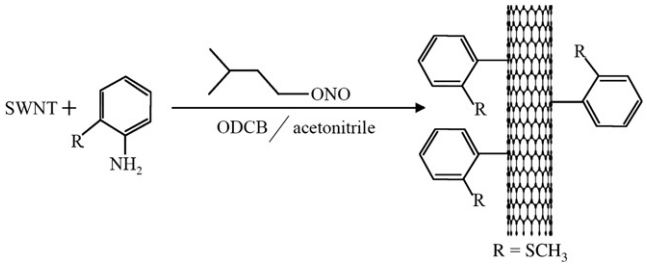

Scheme 1. Functionalization of SWNT with aniline derivative through covalent bonding of diazonium species onto SWNT sidewalls.

2.3. Preparation of nanocomposites

Nanocomposites were prepared by mixing desired amounts of polyisoprene (PI) and SWNTs in toluene at room temperature. Then, thus obtained PI/SWNT suspensions were sonicated for 1 h at the amplitude of 50% and frequency of 1 using homogenizer (Model UP50H, Hielscher Inc.) and then dried in a vacuum oven at room temperature to remove the residual solvent. Sonication was continued while the solvent was being removed in order to improve the dispersion by preventing the precipitation of nanofillers. Identical dispersion methodology was applied to both PISP and PISF, thus affording a quantitative comparison of their dynamics. We reiterate that the codes used throughout the text for nanocomposites with functionalized and pristine nanotubes are PISF and PISP, respectively. A summary of sample descriptions and codes is given in Table 1.

2.4. Techniques

Dielectric measurements were performed on a Novocontrol α high-resolution dielectric analyzer (3 mHz–10 MHz) and a Hewlett–Packard 4291B RF impedance analyzer (1 MHz–1.8 GHz). Both instruments are interfaced to computers and equipped with heating/cooling controls, including Novocontrol's Novocool system custom-modified for measurements at low and high frequency. Dynamic mechanical measurements were conducted using a Rheometrics Scientific's (now TA Inc.) Advanced Rheometric Expansion System (ARES)

Table 1
Sample description and codes

Description	M_w (g mol^{-1})	M_w/M_n	Code	Weight of carbon nanotubes (%)
cis-1,4-Polyisoprene	26,900	1.07	PI	
Pristine single-walled carbon nanotubes			SWNT-p	
Functionalized single-walled carbon nanotubes			SWNT-f	
Composites: PI + SWNT-p			PISP	Varies
Composites: PI + SWNT-f			PISF	Varies

rheometer in the frequency range from 0.01 rad/s to 100 rad/s and temperatures between 223 K and 323 K. A parallel plate (diameter: 8 mm) configuration was employed with a typical gap between the plates of ca. 1.0–1.5 mm. Strain values were selected in the linear viscoelastic range and verified by strain sweeps. Thermogravimetric analysis (TGA) was performed on a TA instrument model TGA–DTA 2960 under nitrogen. Samples were heated from room temperature to 800 °C at a scan rate of 10 °C/min.

3. Results and discussion

3.1. UV spectroscopy and thermal analysis

Characterization of functionalized SWNTs by UV–vis spectroscopy shows a notable effect of functionalization on the absorption spectra, resulting in a surface modification evidenced by comparison of Fig. 1a and b. The absence of the van Hove band structure in the spectrum (Fig. 1b) is indicative of covalent modification [16].

Pristine and functionalized single-walled nanotubes were first tested by thermogravimetric analysis (TGA). The TGA traces show the onset of weight loss at higher temperature for functionalized than pristine SWNTs (Fig. 2a). The improved thermal stability and increased weight loss of PISF nanocomposites (Fig. 2b) may be associated with the enhanced interactions between the PI and the organically modified SWNT sidewalls.

3.2. Dielectric relaxation spectroscopy

Dielectric relaxation spectroscopy (DRS) was performed on a series of nanocomposites containing pristine and functionalized SWNTs at various loadings (%). DRS studies of neat PI are well documented in the literature [17–20] and will not be reviewed here. Suffice it to say that neat PI shows three relaxation processes, termed α_N, α and β, in the order of increasing frequency at constant temperature. The normal mode process (α_N) results from the relaxation of the persistent cumulative dipole moment along the length of type A chains. The time scale and the length scale of the normal mode process vary with molecular weight [19]. We use in this paper the term 'normal mode' to describe the global motion of chains but acknowledge Watanabe's use of a fundamentally more correct term 'eigenmodes' for the relaxation of mathematically well-defined modes [21]. The segmental (α) process is independent of molecular weight [22]. The local (β) process is not explicitly addressed in this study.

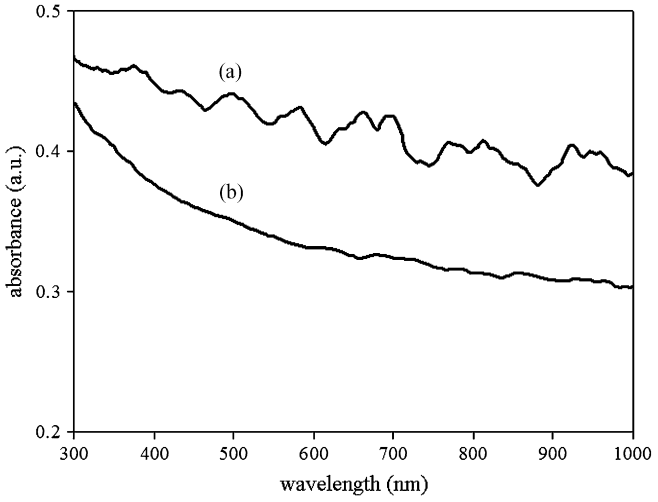

Fig. 1. Absorption spectra of (a) pristine SWNTs and (b) functionalized SWNTs.

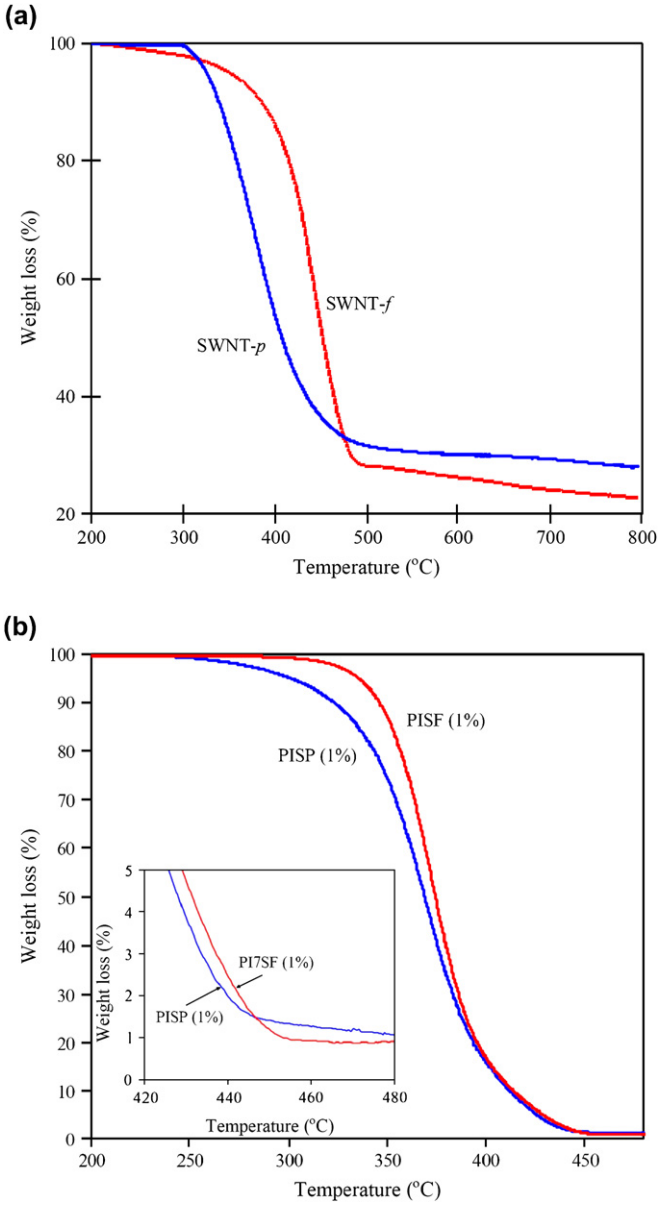

Fig. 2. TGA thermograms of (a) pristine and functionalized SWNTs, and (b) PISP and PISF nanocomposites at 1% loading. Scans were run at 10 °C/min under nitrogen.

We begin by examining how the addition of SWNTs affects the PI dynamics. Fig. 3 shows dielectric loss in the frequency domain for PISP (Fig. 3a) and PISF (Fig. 3b) nanocomposites, respectively. Recall that the sample codes are listed in Table 1. Segmental and normal mode processes in the neat PI, shown

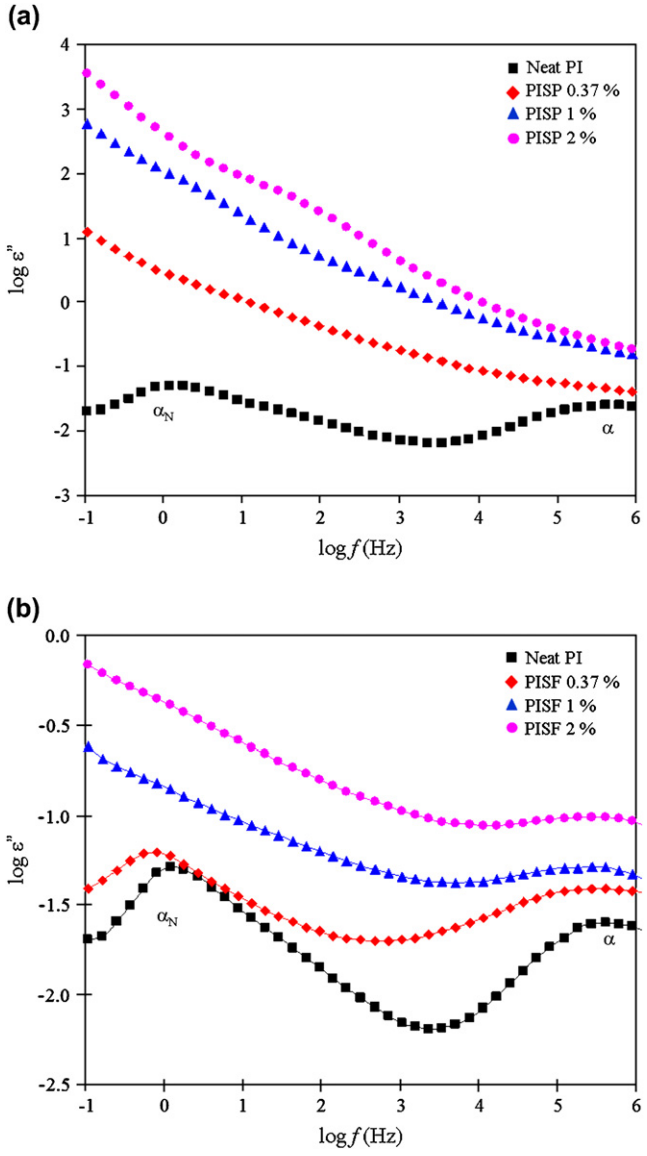

Fig. 3. Dielectric loss in the frequency domain at $T = 253$ K for (a) PISP and (b) PISF nanocomposites with SWNT loading as a parameter.

as reference, are clearly visible in the frequency window of Fig. 3a and b and are marked as α and α_N, respectively. PI has two kinds of dipoles, type A and type B. Type A dipoles are parallel to the chain contour and are relaxed by the motion of entire chain via the normal mode process. Type B dipoles are perpendicular to the chain backbone and are relaxed by segmental motions (the alpha process) [19,23].

As seen in Fig. 3a, the incorporation of pristine single-walled nanotubes (SWNT-p) leads to an increase in the intensity of dielectric loss over the entire frequency window by as much as four orders of magnitude at 2% loading. The normal mode process (α_N) in PISP nanocomposites is largely masked by conductivity but remains visible as a shoulder, marked by an arrow in Fig. 3a. A careful examination of the spectra reveals that the time scale of the α_N process decreases, i.e., shifts to higher frequency, with increasing SWNT-p loading. But despite the strong presence of conductivity, a physically meaningful deconvolution of the loss spectra is possible and the thus obtained values of the average relaxation time are reported later in the text.

A very different picture emerges from the DRS spectra of PISF nanocomposites, shown in Fig. 3b. The increase in loss intensity with increasing SWNT-f loading is much less pronounced here and the normal mode process remains clearly visible at lower loadings. Moreover, we observe an increase in the time scale of the normal mode process in nanocomposites with 0.37 wt% SWNT-f, indicating a decrease in chain mobility. PISF nanocomposites are characterized by better dispersion of SWNT-f in the PI matrix and stronger interactions between these two components due to enhanced compatibility [24–26]. Those interactions, in turn, promote the elongation of PI chains on or near the nanotube surface. The resulting increase in the time scale of the normal mode process is reflected in the shift of the DRS spectra to lower frequency.

Several studies of relaxation near interface have reported a similar effect of matrix–reinforcement interactions on the time scale of the normal mode process. Examples include computational and experimental studies of glass formers in thin films and in porous media. Aoyagi et al. [27] performed a molecular dynamics simulation of polymer melts confined between two solid walls and reported an increase in the normal mode relaxation time with increasing strength of polymer–wall interactions and decreasing distance between the walls. Swenson et al. [28] studied dielectric response of poly(propylene glycol) (PPG) confined to a single molecular layer between clay platelets. They observed a slower normal mode process and ascribed it to surface interactions rather than confinement. Schonhals and Stauga [29] reported a slow down of the whole chain motion of PPG in silanized nanoporous glass and attributed the observed shift to lower frequency to the hydrogen bonding interactions between PPG and hydroxyl groups on the glass surface. Interestingly, this effect is dramatically reduced when a non-chemically treated glass is used. Common to all those reports is the finding that the attractive interactions between the filler surface and the polymer matrix affect the static and dynamic behavior of polymer chains. A direct consequence of adsorption of polymers onto the confining surface is an increase in the time scale of the normal mode process.

The time scale of the segmental process in PISP and PISF nanocomposites is not affected by the addition of nanotubes.

3.2.1. Dielectric modulus formalism

When conductivity dominates the dielectric spectra and masks various relaxation processes, which is particularly common at lower frequencies, the use of the dielectric modulus formalism is often preferred to the permittivity formalism. In such cases, data are expressed in terms of the dielectric modulus, $M^*(\omega)$, defined as the inverse of complex permittivity [23]:

$$M^*(\omega) = M'(\omega) + iM''(\omega) = \frac{1}{\varepsilon^*(\omega)} = \frac{\varepsilon'(\omega) + i\varepsilon''(\omega)}{[\varepsilon'(\omega)]^2 + [\varepsilon''(\omega)]^2} \quad (1)$$

The modulus and permittivity formalisms contain information from the same measurement but differ in the manner in which the underlying dielectric phenomena are suppressed or accentuated. Dielectric modulus spectrum is typically shifted to higher frequency with respect to the permittivity spectrum by a factor related to the ratio of high- and low-frequency limiting permittivity. For the Debye process, the average relaxation times obtained from the modulus (τ_M) and permittivity (τ_ε) formalisms are related according to $\tau_M = (\varepsilon_\infty/\varepsilon_0)\tau_\varepsilon$.

The modulus spectra of nanocomposites offer an added insight into their dynamics because high conductivity makes identification of relaxation processes in the permittivity spectra difficult, though not impossible. Let us examine Fig. 4a, which contains dielectric modulus spectra of neat PI and several PISP nanocomposites with different SWNT-p loading. Neat PI is again shown as reference and normal and segmental relaxations are clearly visible. At 0.37% loading, we observe an increase in the loss modulus intensity and a flattening of the normal mode spectrum over a broad frequency range. With further increase in SWNT-p loading, a broad peak gradually forms, shifts to higher frequency and encroaches on the segmental process, while at the same time another peak emerges at lower frequency. At still higher loading, two relaxation processes become clearly visible in the frequency domain. The dielectric modulus spectra for PISF nanocomposites (Fig. 4b), however, show no such pattern and are very similar to the loss permittivity spectra of Fig. 3b.

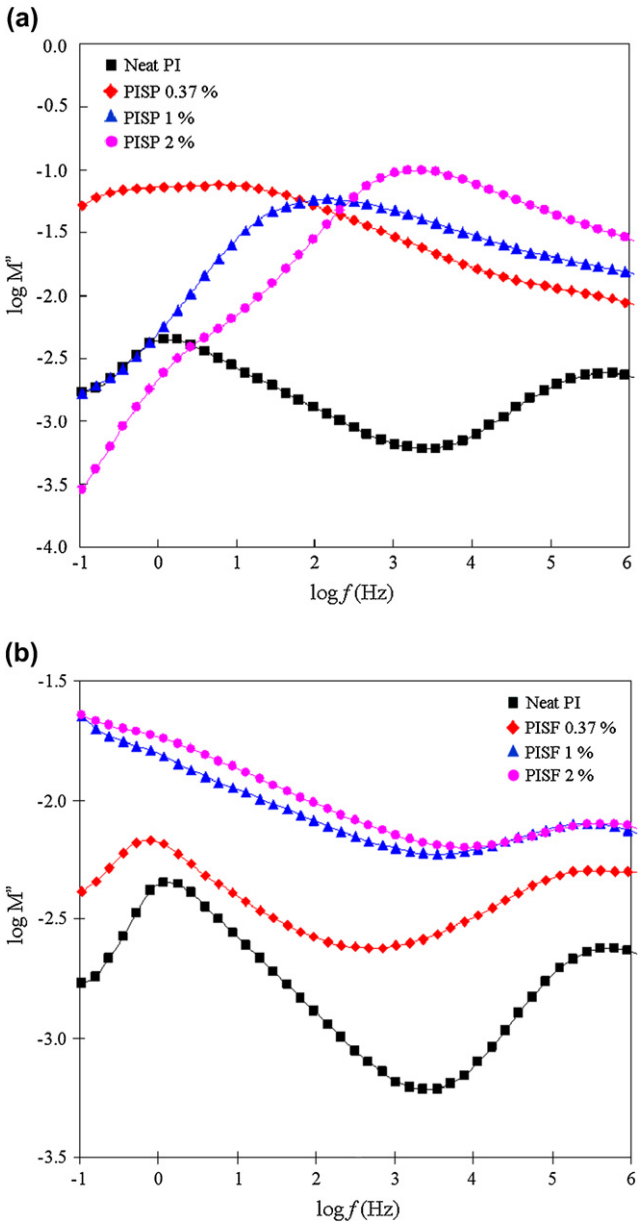

Fig. 4. Dielectric loss modulus in the frequency domain at $T = 253$ K for (a) PISP and (b) PISF nanocomposite with SWNT loading as a parameter.

An interpretation of the dielectric spectra in terms of morphology is of interest. In PISP nanocomposites, pristine nanotubes form bundles or aggregates held together by van der Waals attractive forces. Colloidal dispersions lead to the formation of clusters of aggregates that grow with increasing inorganic content into a cluster network due to the interparticle interactions [30–32]. SWNT-p is largely incompatible with PI and generates agglomerates without limited polymer mediation. PI chains confined within the agglomerates will assume a non-elongated conformation due to weak interactions with SWNT-p, resulting in a reduced effective length scale and a faster response to the applied electric field. Floudas et al. [33] studied the normal mode processes in *cis*-PI confined to nanoporous glass. They reported faster relaxation in untreated pores and attributed it to the weak interactions and confinement of PI chains. But in the trimethylsilyl treated pores they observed slower relaxation because of the strong interactions between the chemically modified glass surfaces and PI. The shift of relaxation peak to higher frequency with increasing SWNT-p loading also suggests that the number density of confined PI chains increases due to the larger network of SWNT-p agglomerates.

Dielectric loss modulus in the frequency domain with temperature as a variable is shown in Fig. 5a and b, for PISP (1%) and PISF (1%), respectively. It is immediately evident from Fig. 5a that an increase in temperature has a very well-defined and reproducible effect on the spectra of PISP nanocomposites. Fig. 5a clearly illustrates the systematic shift of a broad peak to higher frequency with increasing temperature and a simultaneous emergence of an additional peak in the lower frequency region. The broad peak represents the normal mode process while the lower-intensity, low-frequency peak is due to the Maxwell–Wagner–Sillars (MWS) polarization caused by the charge accumulation along the SWNT/PI interface. These two processes are also visible in the dielectric modulus spectra of PISF nanocomposites, shown in Fig. 5b, but with a dramatically different result. Here, the intensity of the MWS polarization far exceeds that of the normal mode process. A better dispersion of SWNT-f in the nanocomposites gives rise to a larger interfacial area, which, in turn, leads to a higher degree of charge accumulation along the interface.

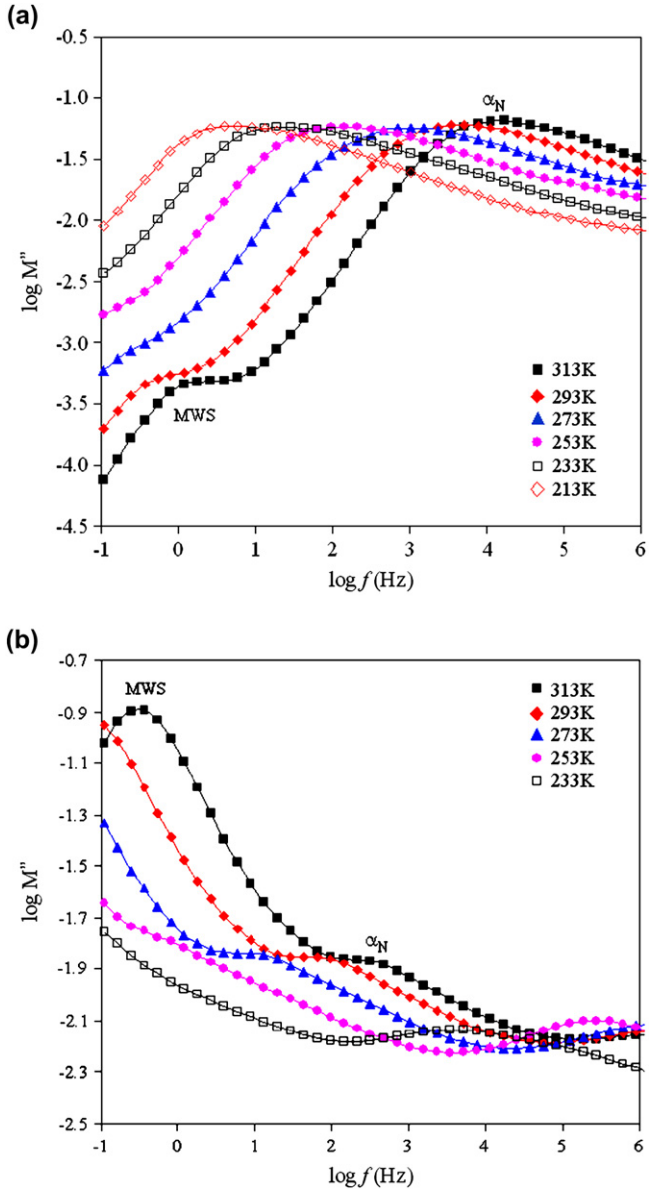

Fig. 5. Dielectric loss modulus in the frequency domain with temperature as a variable for (a) PISP and (b) PISF nanocomposite at 1% loading.

3.2.2. Temperature dependence of average characteristic time

We note that in the remainder of the text we define the average relaxation time for the segmental and normal mode process in PISP and PISF nanocomposites as the reciprocal angular frequency at maximum loss in the dielectric permittivity spectra. A deconvoluted dielectric spectrum for PISP (1%) is shown in Fig. 6. Notwithstanding the conductivity contribution, three processes are visible and the spectrum is conducive to a physically meaningful deconvolution. In the order of increasing frequency we observe the MWS polarization, the normal mode process and the segmental process. The values of τ_{MWS}, τ_N and τ_s were obtained from the fits to the well-known Havriliak–Negami (HN) functional form. The temperature dependence of the average relaxation time for the normal (τ_N) and segmental (τ_s) mode process is plotted in Fig. 7a and b,

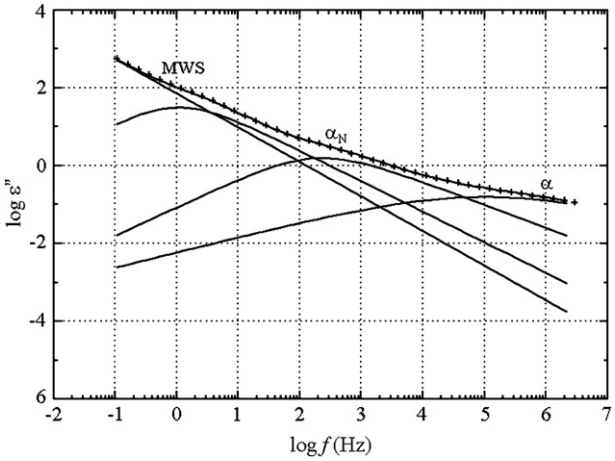

Fig. 6. Dielectric loss in the frequency domain for PISP (1%) at $T = 253$ K. The spectrum was deconvoluted into three separate relaxation modes (MWS, normal and segmental).

for PISP and PISF, respectively. We note that normal and segmental relaxations in all nanocomposites exhibit the Vogel–Fulcher–Tammann (VFT) temperature dependence, but that is where the similarities in the normal mode relaxation in PISP and PISF end. An increase in nanotube loading has the exact opposite effect on the time scale of the normal mode process in PISP and PISF nanocomposites. As seen in Fig. 7a, the time scale of the normal mode process in PISP *decreases* with increasing loading as the role of confined PI chains becomes more significant with increasing agglomeration of SWNT-p. In PISF, however, the time scale of the normal mode process *increases* with increasing SWNT-f loading (Fig. 7b). We attribute this phenomenon to increased interactions between SWNT-f and the matrix that leads to the elongation of PI chains along the nanotubes and a concomitant decrease in their mobility. Interestingly, however, the chain mobility appears to level off at about 2% loading and does not decrease beyond that value. As the number density of SWNT-f increases, the average interaction energy decreases and we actually observe a reverse trend in dynamics. The segmental process in PISP and PISF does not show notable deviation from the neat PI suggesting limited effect of nanotubes on segmental motions.

3.2.3. Conductivity

We begin this section by pointing out that the frequency dependence of conductivity can be expressed by a sum of the dc component and the frequency power law terms according to [34,35]:

$$\sigma(\omega) = \sigma_{dc} + \sum_i A_i \omega^{s_i} \tag{2}$$

where σ_{dc} is dc conductivity, A_i is temperature dependent parameter in ith frequency domain and s_i is the frequency exponent in ith frequency domain. The exponent s is obtained by fitting Eq. (2) for each frequency domain. For our samples, exponent s lies between 0.1 and 1.0 throughout the entire

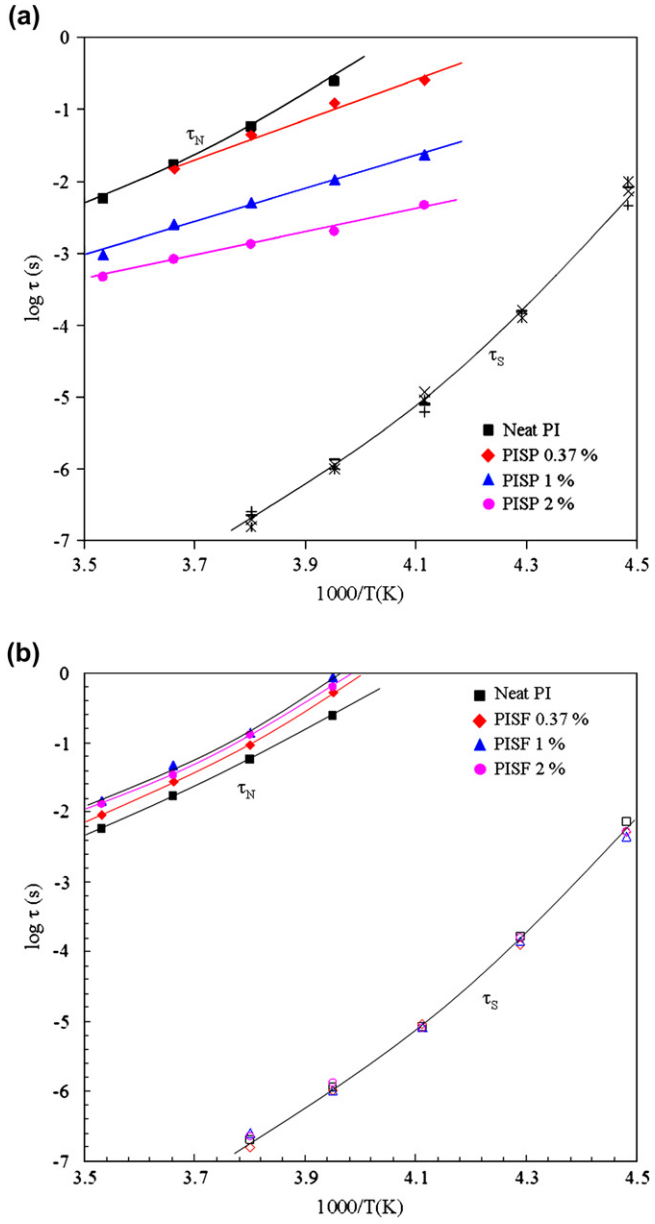

Fig. 7. Temperature dependence of the average relaxation time for the normal mode (τ_N: solid symbols) and segmental mode (τ_s: open symbols) with SWNT (wt%) as a parameter for (a) PISP and (b) PISF.

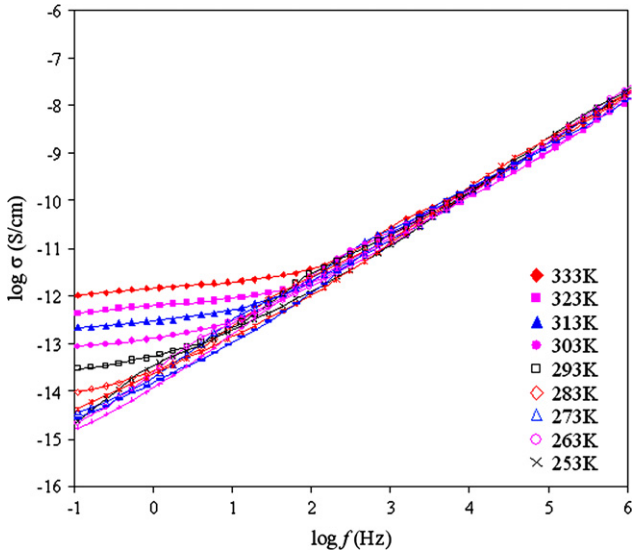

Fig. 8. Conductivity in the frequency domain for PISF (0.37%) nanocomposite with temperature as a variable.

frequency range. Fig. 8 illustrates conductivity in the frequency domain with temperature as a variable. It is evident that the conductivity spectra are characterized by frequency independent dc (ionic) region at low-frequency and a frequency dependent region – above some critical (f_c) frequency [36–38]. We stress that conductivity in the frequency dependent region does not necessarily follow only one straight line and that is accounted for by the inclusion of more than one power term under the summation sign in Eq. (2). Fig. 8 also shows how the dc conductivity domain becomes progressively smaller with decreasing temperature and vanishes at about 273 K [39,40]. Conversely, the transition frequency (f_t) shifts to higher frequency with increasing temperature. Ishii et al. reported that the exponent s was typically greater than 1 at lower frequencies and less than 1 at higher frequencies [41]. In our PISP nanocomposite, s varies between 0.1 and 0.6 at higher frequencies and increases to about 1.0 at lower frequency. But in the case of PISF nanocomposite, s remains constant at approximately 1.0 over the entire frequency range, independent of SWNT-f loading.

Fig. 9 illustrates the effect of SWNT-p (Fig. 9a) and SWNT-f loading (Fig. 9b) on conductivity at $T = 253$ K. It is readily seen that conductivity increases with increasing loading in all nanocomposites. But a much more pronounced increase in conductivity with loading is observed in PISP nanocomposites, as seen in Fig. 9a, due to the build-up of an electrical charge pathway through the network of agglomerated SWNT-p in the PI matrix [42,43]. A less pronounced increase in conductivity with increasing loading in PISF, seen in Fig. 9b, points out to the role of covalent functionalization in reducing the electrical conductivity of isolated nanotubes because the initial sp^2 hybridized electronic state of SWNT is converted to the more resistive sp^3 configuration due to the ligand attachment on the side walls [44].

The temperature dependence of dc conductivity is Arrhenius-like and given by

$$\sigma_{dc} = \sigma_0 \exp\left(-\frac{E}{kT}\right) \tag{3}$$

where σ_{dc} is dc conductivity, σ_0 is a constant, E is an activation energy and k is the Boltzmann constant. The temperature dependence of dc conductivity in PISP and PISF is plotted in Fig. 11a and b, respectively. The value of dc conductivity was obtained by extrapolation of the frequency independent region to $\omega \to 0$. As shown in Fig. 10a, dc conductivity increases with increasing SWNT-p loading and the activation energy calculated from Eq. (3) decreases from 0.414 eV at 0.37% to 0.255 eV at 2% loading. Analogous trend, although at a much smaller scale, is seen in PISF (Fig. 10b).

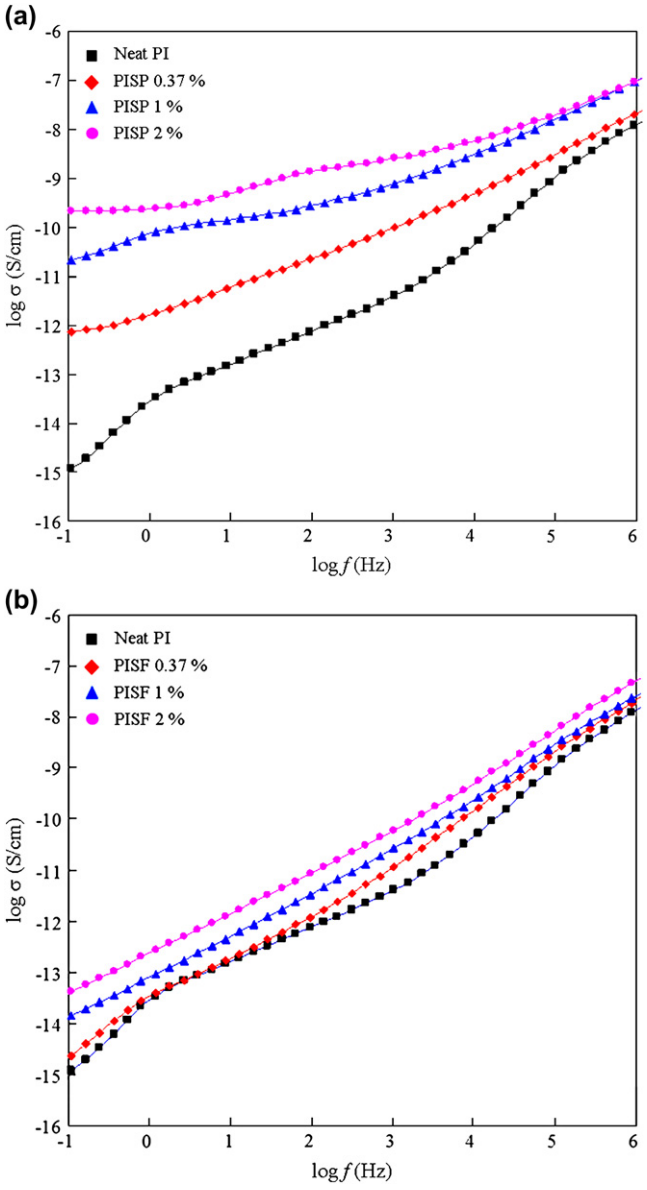

Fig. 9. Conductivity in the frequency domain with SWNT (wt%) as a parameter for (a) PISP and (b) PISF nanocomposites.

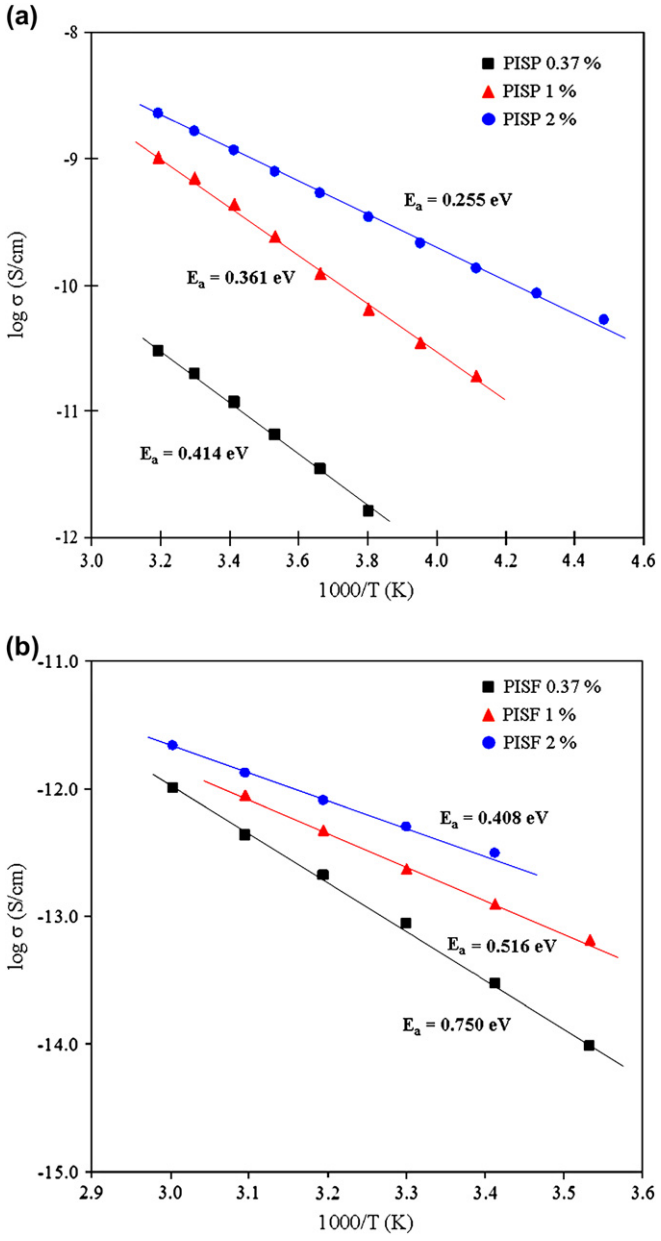

Fig. 10. dc Conductivity as a function of reciprocal temperature with SWNT (wt%) as a parameter for (a) PISP and (b) PISF nanocomposites.

3.3. Dynamic mechanical spectroscopy

In this section, we describe the rheology of nanocomposites as studied by dynamic mechanical spectroscopy (DMS). Strain amplitude was determined to be within the linear viscoelastic region by dynamic strain sweeps. Master curves were generated from the time–temperature superposition of isothermal frequency sweeps using the horizontal (frequency) shift factor a_T, with respect to the reference temperature. The results for PISP and PISF nanocomposites are shown in Fig. 12a and b, respectively. The difference in the DMS response of PISP (Fig. 11a) and PISF (Fig. 11b) is notable. The master curves in Fig. 11a show that the addition of SWNT-p causes a small increase in the plateau modulus but has little effect on the slope of the storage modulus (G') in the low-frequency region. Only at the SWNT-p loading of 5% we observe a weak shoulder in the terminal zone – a sign of pseudo solid-like behavior [45]. Pristine nanotubes do not contribute significantly to the reinforcement of nanocomposites due to their weak interactions with PI chains and a poor dispersion within the matrix. A very different result was obtained for PISF nanocomposites, as seen in Fig. 11b. An increase in SWNT-f loading triggers a considerable increase in G' in the terminal zone. In PISF nanocomposites, the low-frequency value of G' increases while its slope decreases with increasing loading. Neat PI displays liquid-like characteristics of a Newtonian fluid with near terminal behavior ($G' \sim \omega^2$) [46]. With increasing SWNT-f loading, we observe a sharp decrease in the ω dependence of G' in the terminal region. At 5% loading G' approaches a low-frequency plateau indicative of the

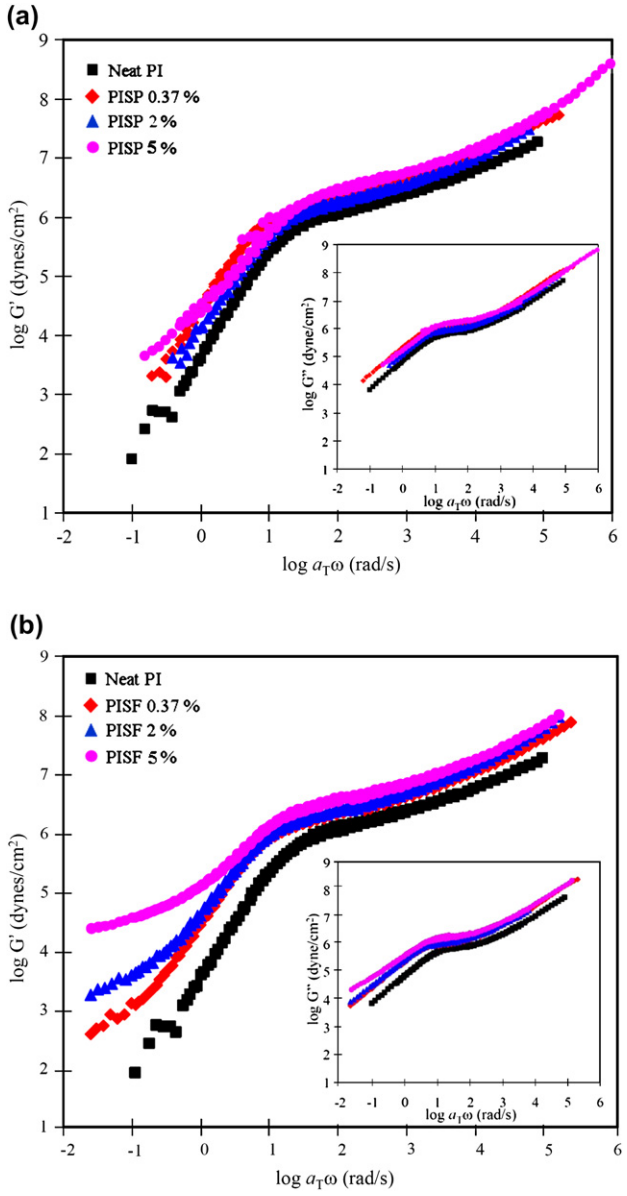

Fig. 11. Time–temperature superposed dynamic storage modulus G' for (a) PISP and (b) PISF with SWNT (wt%) as a parameter at $T_0 = 253$ K.

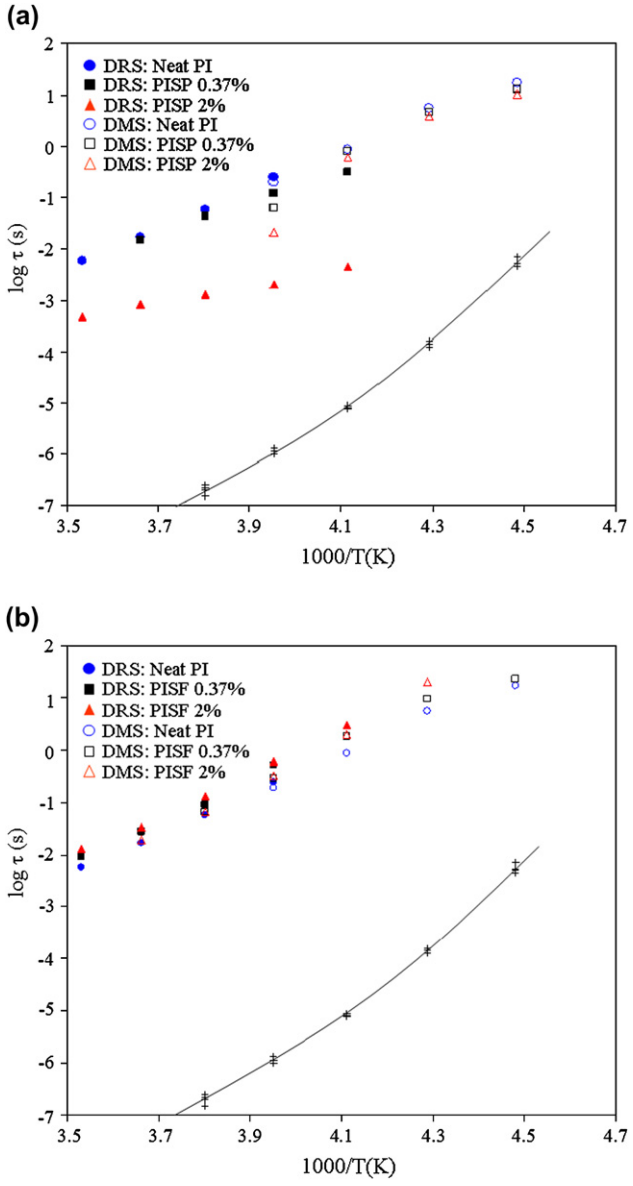

Fig. 12. Temperature dependence of the relaxation time for the normal mode process with SWNT loading as a parameter in (a) PISP and (b) PISF. Filled and open symbols represent DRS and DMS measurements, respectively. DRS segmental mode (cross) is shown for reference.

pseudo solid-like viscoelastic response [47]. Uchida and Kumar [48] reported improved mechanical properties when nanotubes were fully exfoliated in the matrix and showed that composites containing bundles did not possess enhanced strength. A molecular simulation study by Liab and Li [49] of carbon nanotube (CNT)–polystyrene composites shows that the enhancement of mechanical properties depends on the fiber–matrix interfacial shear stress resulting from the intimate contact between the CNTs and the polymer matrix. The functionalization of SWNTs affects the interactions between the polymer matrix and the nanotubes by inducing a better dispersion and, ultimately, by imparting enhanced mechanical properties to nanocomposites. An additional indicator of better dispersion of nanotubes in the composite is the higher value of G' or a lower slope in the terminal zone observed in the DMS spectra [4].

The terminal relaxation time calculated from the DMS data (τ_1), using the relationship $\tau_1 = \eta_0/G_N$, is compared with the DRS result (τ_ε) in Fig. 13a and b. Zero-shear viscosity (η_0) was obtained from the data by averaging the low shear rate values of η. The plateau modulus (G_N) was determined by taking the value of the onset of transition from segmental to terminal mode [50,51]. The time scale of the terminal relaxation in PISP decreases with increasing loading, as seen in Fig. 12a. But despite analogous trends, the values calculated from DRS and DMS data for PISP nanocomposites are not in consistently good agreement at all loadings. For example, at SWNT-p loading of 0.37%, the DMS and DRS results coincide. With increasing loading, however, the difference between τ_N and τ_1 becomes larger, due to the poor dispersion of SWNT-p in

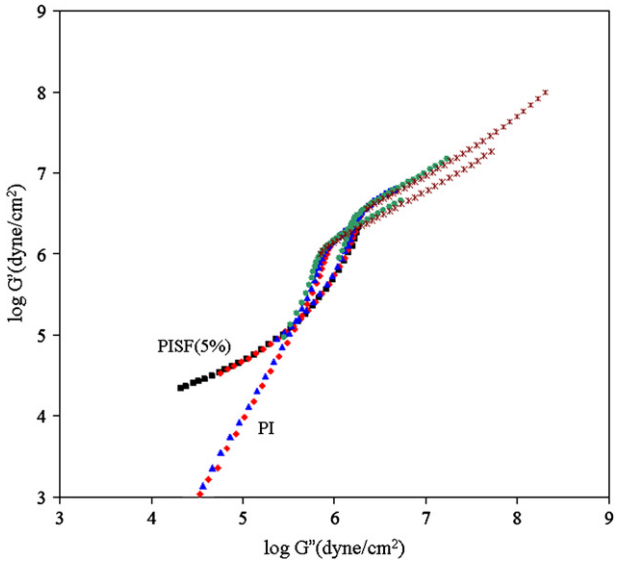

Fig. 13. $G'-G''$ plot for neat PI and PISF (5%).

the PI matrix. An explanation of the discrepancy between DRS and DMS results is rationalized as follows. PI in PISP nanocomposites is present partly as bulk phase and partly as confined phase between the SWNT-p agglomerates. DRS measurement is sensitive to both phases, resulting in the observed shift in the relaxation spectrum to higher frequency, i.e., faster relaxation. DMS measurements, on the other hand, capture a macroscopic response of the nanocomposite and that may account for the observed discrepancy.

In PISF nanocomposites, however, the increase in the time scale of terminal relaxation with increasing SWNT-f loading is consistent with the DRS results, as seen in Fig. 12b. The uniform dispersion of carbon nanotubes, aided by functionalization, is conducive to yielding a similar length scale and time scale of PI dynamics as measured by DRS and DMS.

A $G'-G''$ plot for neat PI and PISF (5%) in the temperature range from 223 K to 263 K is presented in Fig. 13. In that temperature range, both samples are thermorheologically simple and the modulus shift factor b_T (vertical shifting) is not required for time–temperature superposition [52]. A lower G' of PISF (5%) in the intermediate temperature range is the consequence of a more viscous nature of PISF (5%) compared to PI. However, a higher G'/G'' ratio in PI does not imply that the storage modulus (G') of PI is higher than that of PISF (5%) in this temperature range. At the low temperature end of the plot, the PISF (5%) nanocomposite loading has a higher storage modulus, suggesting that better reinforcement is facilitated by the PI matrix.

4. Conclusions

We have completed an investigation of dynamics of single-walled carbon nanotube (SWNT)/polyisoprene (PI) nanocomposites by a combined use of dielectric relaxation spectroscopy (DRS) and dynamic mechanical spectroscopy (DMS). Surface treatment of nanotubes is important to dynamics as evidenced by the difference in the normal mode relaxation in nanocomposites with pristine (PISP) and functionalized (PISF) SWNTs. Reproducibility and reliability of results were established through careful sample preparation and verified through repeated measurements.

PISF nanocomposites are characterized by strong interfacial interactions that increase the time scale of the normal mode process and increase the storage modulus in the terminal zone but slow down the increase in conductivity. An increase in SWNT-f loading triggers a considerable increase in G' and at 5% loading we observe a low-frequency plateau indicative of the pseudo solid-like viscoelastic response. We also note excellent agreement in the average relaxation time for the normal mode process calculated from DRS and DMS data and that is due to good dispersion of SWNT-f in the polymer matrix.

PISP nanocomposites show the opposite trend and we observe a faster normal mode process with increasing SWNT-p loading. A scenario was advanced whereby the PI chains in PISP nanocomposites are partitioned between bulk and confined domains. The observed decrease in the time scale of normal mode relaxation is envisioned as a consequence of the strong effect on dynamics of the PI chains that are confined within the SWNT-p agglomerates. PISP nanocomposites are characterized by a difference in the average relaxation time for the normal mode process as measured by DRS and DMS, and this discrepancy is attributed to the fact that the DRS spectra are affected by the presence of the confined PI phase whereas the DMS measurement captures the bulk response. Finally, pristine nanotubes do not contribute significantly to the storage modulus in the terminal zone due to their weak connectivity with PI and a poorer dispersion within the matrix.

Acknowledgement

This material is based on work supported by National Science Foundation under Grant DMR-0346435.

References

[1] Jang J, Bae J, Yoon SH. J Mater Chem 2003;13:676–81.
[2] Allaoui A, Bai S, Cheng HM, Bai JB. Comp Sci Tech 2002;62l:1993–8.
[3] Ajayan PM, Stephan O, Colliex C, Trauth D. Science 1994;265:1212–4.
[4] Moniruzzaman M, Winey KI. Macromolecules 2006;39:5194–205.
[5] Ramanathan T, Liu H, Brinson LC. J Polym Sci Part B Polym Phys 2005;43:2269–79.
[6] Zhu J, Kim J, Peng H, Margrave JL, Khabashesku VN, Barrera EV. Nano Lett 2003;3:1107–13.
[7] Zhang X, Liu T, Sreekumar TV, Kumar S, Moore VC, Hauge RH, et al. Nano Lett 2003;3:1285–8.
[8] Wang Z, Liu Q, Zhu H, Liu H, Chen Y, Yang M. Carbon 2007;45:285–92.
[9] Zhang W, Joshi A, Wang Z, Kane RS, Koratkar N. Nanotechnology 2007;18:185703–7.
[10] Putz KW, Mitchell CA, Krishnamoorti R, Green PF. J Polym Sci Part B Polym Phys 2004;42:2286–93.
[11] Kim JA, Seong DG, Kang TJ, Youn JR. Carbon 2006;44:1898–905.
[12] Bahr JL, Yang J, Kosynkin DV, Bronikowski MJ, Smalley RE, Tour JM. J Am Chem Soc 2001;123:6536–42.
[13] Qin S, Qin D, Ford WT, Resasco DE, Herrera JE. Macromolecules 2004;37:752–7.

[14] Mitchell CA, Bahr JL, Arepalli S, Tour JM, Krishnamoorti R. Macromolecules 2002;35:8825–30.
[15] Dyke CA, Tour JM. J Am Chem Soc 2003;125:1156–7.
[16] Bahr JL, Tour JM. J Mater Chem 2002;12:1952–8.
[17] Boese D, Kremer F. Macromolecules 1990;23:829–35.
[18] Yoshida H, Adachi K, Watanabe H, Kotaka T. Polym J 1989;21:863–70.
[19] Imanishi Y, Adachi K, Kotaka T. J Chem Phys 1988;89:7585–92.
[20] Doxastakis M, Theodorou DN, Fytas G, Kremer F, Faller R, Plathe FM. J Chem Phys 2003;119:6883–94.
[21] Watanabe H. Macromol Rapid Commun 2001;22:127–75.
[22] Mijovic J. In: Kremer F, Schonhals A, editors. Broadband dielectric spectroscopy. Berlin: Springer-Verlag; 2003. p. 349–84 [chapter 9].
[23] Kremer F, Schonhals A. Broadband dielectric spectroscopy. Berlin: Springer-Verlag; 2003.
[24] Feijoo J, Cabedo L, Gimenez E, Lagaron J, Saura J. J Mater Sci 2005;40:1785–8.
[25] Hu N, Zhou H, Dang G, Rao X, Chen C, Zhang W. Polym Int 2007;56:655–9.
[26] Hadjiev VG, Mitchell CA, Arepall S, Bahr JL, Tour JM, Krishnamoorti R. J Chem Phys 2005;122:124708–13.
[27] Aoyagi T, Takimoto J, Doi M. J Chem Phys 2001;115:552–9.
[28] Swenson J, Schwaltz GA, Bergman R, Howells WS. Eur Phys J E 2003;12:179–83.
[29] Schonhals A, Stauga R. J Chem Phys 1998;108:5130–6.
[30] Meakin P. Phys Rev Lett 1983;51:1119–22.
[31] Kolb M, Botet R, Julien R. Phys Rev Lett 1983;51:1123–6.
[32] Paiva MC, Zhou B, Fernando KAS, Lin Y, Kennedy JM, Sun YP. Carbon 2004;42:2849–54.
[33] Petychakis L, Floudas L, Fleischer G. Europhys Lett 1997;40:685–90.
[34] Bisquert J, Garcia-Belmonte G. Russ J Electrochem 2004;40:352–8.
[35] Narula AK, Singh R, Chandra S. Bull Mater Sci 2000;23:227–32.
[36] Hindermann-Bischoff M, Ehrburger-Dolle F. Carbon 2001;39:375–82.
[37] Kim YJ, Shin TS, Choi HD, Kwon JH, Chung YC, Yoon HG. Carbon 2005;43:23–30.
[38] Rimska Z, Kresalek V, Spacek J. Polym Comp 2002;23:95–103.
[39] De S, Dey A, De SK. Eur Phys J B Condens Matter Phys 2005;46:355–61.
[40] Dey A, De S, De A, De SK. Nanotechnology 2004;15:1277–83.
[41] Ishii T, Abe T, Shirai H. Solid State Commun 2003;127:737–41.
[42] Tamburri E, Orlanducci S, Terranova ML, Valentini F, Palleschi G, Curulli A, et al. Carbon 2005;43:1213–21.
[43] Potschke P, Fornes TD, Paul DR. Polymer 2002;43:3247–55.
[44] Farmer DB, Gordon RG. Electrochem Solid-State Lett 2005;8:G89–91.
[45] Mijovic J, Lee HK, Kenny J, Mays J. Macromolecules 2006;39:2172–82.
[46] Ren J, Silva AS, Krishnamoorti R. Macromolecules 2000;33:3739–46.
[47] Shi X, Hudson JL, Spicer PP, Tour JM, Krishnamoorti R, Mikos AG. Nanotechnology 2005;16:S531–8.
[48] Uchida T, Kumar SJ. Appl Polym Sci 2005;98:985–9.
[49] Liab K, Li S. Appl Phys Lett 2001;79:4225–7.
[50] Mijovic J, Han Y, Sun M. Macromolecules 2002;35:6417–25.
[51] Mijovic J, Sun M, Pejanovic S, Mays JW. Macromolecules 2003;36:7640–51.
[52] Zarraga A, Pena JJ, Munoz ME, Santamaria A. J Polym Sci Part B Polym Phys 2000;38:469–77.